THE JOURNAL OF PHYSICAL CHEMISTRY B

ARTICLE

pubs.acs.org/JPCB

Role of Arg82 in the Early Steps of the Bacteriorhodopsin Proton-Pumping Cycle

Maike Clemens,[†] Prasad Phatak,[‡] Qiang Cui,[§] Ana-Nicoleta Bondar,[∥] and Marcus Elstner*[,⊥]

[†]Department of Theoretical and Computational Biophysics, Max-Planck-Institute for Biophysical Chemistry, Am Fassberg 11, 37077 Göttingen, Germany

[‡]Department of Chemistry, Indiana University, 800 E Kirkwood Avenue, Bloomington, Indiana 47405, United States

[§]Department of Chemistry and Theoretical Chemistry Institute, University of Wisconsin, Madison, 1101 University Avenue, Madison, Wisconsin 53706, United States

[∥]Department of Physiology and Biophysics and Center for Biomembrane Systems, University of California at Irvine, Med. Sci. I, D-347, Irvine, California 92697, United States

[⊥]Theoretical Chemical Biology, Karlsruhe Institute of Technology (KIT) Institute of Physical Chemistry, Kaiserstrasse 12, 76131 Karlsruhe, Germany

Supporting Information

ABSTRACT: Proton-transfer reactions in the bacteriorhodopsin light-driven proton pump are coupled with structural rearrangements of protein amino acids and internal water molecules. It is generally thought that the first proton-transfer step from retinal Schiff base to the nearby Asp85 is coupled with movement of the Arg82 side chain away from Asp85 and toward the extracellular proton release group. This movement of Arg82 likely triggers the release of the proton from the proton release group to the extracellular bulk. The exact timing of the movement of Arg82 and how this movement is coupled with proton transfer are still not understood in molecular detail. Here, we address these questions by computing the free energy for the movement of the Arg82 side chain. The calculations indicate that protonation of Asp85 leads to a fast reorientation of the Arg82 side chain toward the extracellular proton release group.

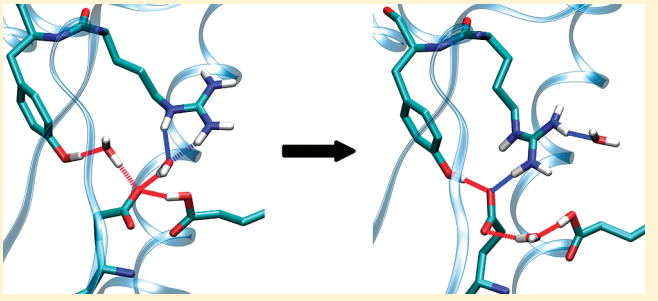

I. INTRODUCTION

Bacteriorhodopsin, a light-driven proton pump found in the purple membrane of the archeaon *Halobacterium salinarum*,[1,2] consists of seven transmembrane helices with the retinal chromophore covalently bound through a protonated Schiff base (PSB) to Lys216 on helix G (Figure 1). The proton-pumping reaction cycle of bacteriorhodopsin is initiated after retinal's light-induced isomerization from the all-trans configuration in the bR resting state to the 13-cis configuration.[3,4] The reaction cycle consists of the passage through the intermediate states bR, K, L, M, N, and O, characterized by their UV−vis absorption maxima.[5] The first proton-transfer step, from the Schiff base to the nearby Asp85, occurs during the L-to-M transition; during the lifetime of M, another proton is released to the extracellular bulk from the so-called proton release group (PRG). The net effect of one reaction cycle is translocation of one proton from the cytoplasm to the extracellular bulk. Arg82 is located approximately at the middle of the extracellular proton release pathway (Figure 1). In the bR resting state, the side chain of Arg82 points toward the Schiff base (red structure in Figure 2),[6] acting as a gate that hinders direct access of extracellular bulk water molecules to the Schiff base region; a similar geometry of Arg82 is also observed in K state.[7] The location of the internal water molecules in the bR resting state is shown in Figure 3. The bR resting state is characterized by a pentagonal hydrogen-bonded network (HBN). This network includes the protonated Schiff base; the negatively charged Asp85 and Asp212; water molecules w401, w402, and w406; and Thr89; Asp212 further hydrogen-bonds to Tyr57 (Figure 3). Although the Schiff base is oriented toward Asp212 in K,[7−11] the amino acid side chains and the water molecules remain part of the HBN. The pentagonal HBN is no longer observed in the late-M state. Crystal structures of the M state indicate one[12] or two[13] water molecules in the region occupied by the pentagonal HBN in the bR state.

The geometry of the Arg82 side chain in the pre-proton-transfer state L is controversial (Figure 3). Of the five crystal structures proposed for L,[14−16] three indicate a geometry of Arg82 similar to that in the bR resting state, and two structures

Received: February 25, 2011
Revised: April 13, 2011
Published: May 11, 2011

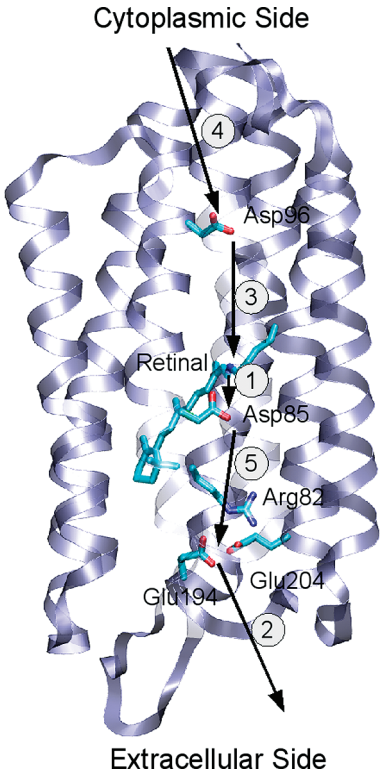

Figure 1. Five proton-transfer steps in the bR proton-pumping cycle. In the bR resting state, retinal is all-trans, the Schiff base is protonated, and Asp85 negatively charged; Asp115, Asp96, and the PRG are protonated.

indicate Arg82 pointing toward the extracellular side.[17,18] The L-state structures of refs 17 and 18 might be due to the crystal containing a mixture of L and M. Conflicting information on the geometry of Arg82 is also provided by the crystal structures of the M substates. In structures proposed for the early-M state (i.e., the M state immediately after Schiff-base deprotonation), Arg82 points toward the Schiff base region.[19,20] In contrast, Arg82 is oriented toward the PRG in the late-M state, as indicated by the blue structure in Figure 2.[12,13] The geometry of Arg82 in the crystal structures of the bR, K, L, and M intermediate states suggests that the movement of Arg82 is somehow coupled to the proton-transfer events. pK_a studies on R82K mutants have suggested that the pK_a of Asp85 is controlled by the positive charge at Arg82, and Arg82 might also be a part of the proton release complex at the extracellular side.[21] However, the exact timing of the movement and the nature of the coupling remain unclear.

Site-directed mutagenesis experiments indicate that, in addition to the positive charge, the Arg side chain at position 82 is necessary for an optimal reaction cycle: the pK_a of the PRG during the L-to-M transition is lowered (and the proton released) not only in Arg82His, but also in the Arg82Gln mutant.[22] The much slower proton transfer from Asp85 to the PRG in the O-to-bR transition of Arg82His as compared to the wild type further supports an important functional role of Arg82.[23] Multiconformation equilibrium electrostatics computations suggested that Arg82, when oriented toward the Schiff base region, stabilizes the zwitterionic state with protonated Schiff base and negatively charged Asp85. In contrast, when oriented toward the PRG, Arg82 stabilizes the unprotonated Schiff base/protonated Asp85 (M-like) state and the deprotonated state of the PRG.[24]

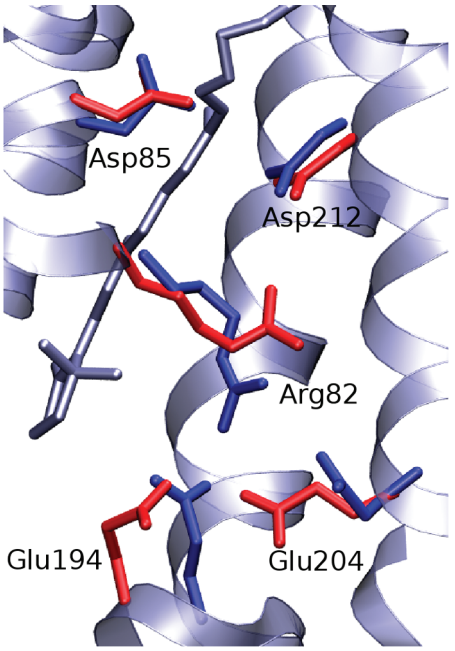

Figure 2. Proton transfer is associated with reorientation of the Arg82 side chain from the cytoplasmic side in the preproton-transfer state (red structure) to the extracellular side in the M state (blue). The PRG consists of Glu194/Glu204 and nearby water molecules. The crystal structure of the L state[16] (red) is compared to that of the late-M state[13] (blue).

To investigate the coupling between the movement of Arg82 and the proton-transfer steps, we performed classical molecular dynamics (MD) simulations and free energy computations on an early-M-like structure. The results indicate that the transfer of the proton from the retinal Schiff base to Asp85 triggers rapid movement of Arg82 toward the PRG.

II. METHODS

A. Preparation of the Structure Used for Computations. Crystal structures indicate very similar geometries of the protein in the bR, K, L, and early-M intermediates.[25,26] To avoid the controversies over structural details of L, we used the K-state crystal structure[27] for the starting protein coordinates. The protein atoms were described with the all-atom CHARMM force field for proteins,[28] and the water molecules were described with the TIP3P model.[29] Asp115 and Asp96 were considered protonated.[30,31] Asp85 is negatively charged in the pre-proton-transfer states bR, K, and L states and neutral with neutral Schiff base in M state.[30,31] Glu204 of the PRG is protonated, and Glu194 is negatively charged.[32] Note that a quantum mechanics/molecular mechanics (QM/MM) treatment of the PRG leads to a delocalization of the proton between Glu194 and Glu204. For classical simulations, however, a protonation of one of the residues will lead to overall similar electrostatic interactions. Hydrogen atoms were constructed using the HBUILD facility[33] of the CHARMM software.[28,34]

For classical MD simulations, the partial charges of the retinal with unprotonated Schiff base were obtained from benchmark self-consistent-charge density-functional tight-binding (SCC-DFTB)/CHARMM calculations in which the retinal was treated at the SCC-DFTB level (see the Supporting Information).

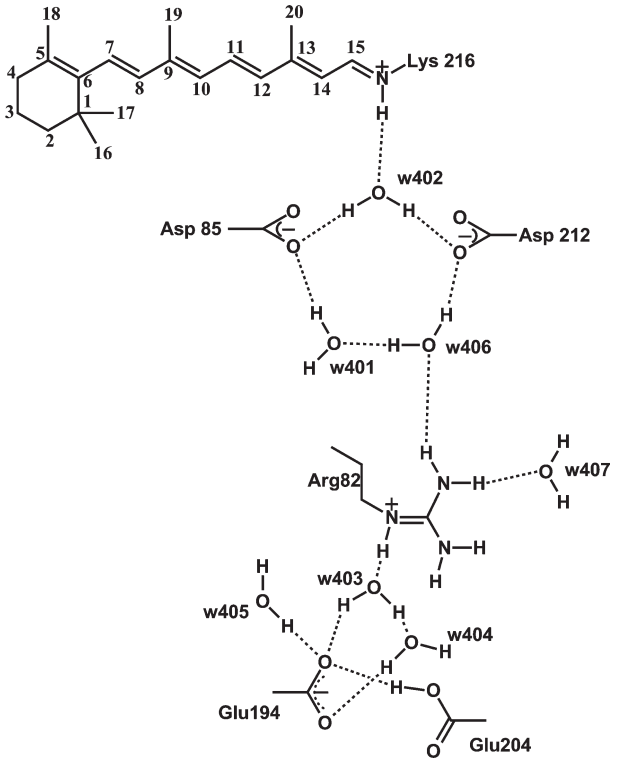

Figure 3. Schematic representation of the HBN in the extracellular half of bacteriorhodopsin bR (ground) state. The scheme was prepared based on the crystal structure from ref 6. Similar geometries of the internal water molecules and Arg82 are indicated by the K-state crystal structures of refs 7 and 11. The location of w402 in L is controversial.[16,26,49,50] Arg82 is oriented toward the Schiff base in all crystal structures of the early photocycle steps, except for the L-state structure of refs 17 and 18.

B. Stochastic Boundary Setup. In all simulations, the long-range electrostatic effects were modeled using the generalized solvent boundary potential (GSBP) approach[35] as implemented for QM/MM models in CHARMM.[36] In all cases, the system was partitioned into a 22-Å inner region centered at N_ε atom of Arg82, whereas the rest was treated as the outer region within the framework of the GSBP approach.[35] Newtonian equations of motion were solved for the MD region (within 18 Å), and Langevin equations of motion were solved for the buffer region (18−22 Å) with a temperature bath of 300 K.[37] All water molecules in the inner region were subjected to a weak GEO (geometric) type of restraining potential to keep them inside the inner sphere with the MMFP (miscellaneous mean field potential) module of CHARMM. The GEO restraining potential is in the form of a quartic polynomial on each oxygen atom in water, namely, $k\Delta^2(\Delta^2 - V_P)$, with $\Delta = r - r_{off}$, where k is the restraining quartic force constant [0.5 kcal/(mol·Å^4)], r is the distance of the oxygen from the center of the simulation sphere, r_{off} is the cutoff distance (22.0 − 1.5 = 20.5 Å) below which the GEO restraint is set to zero, and V_P is an offset value taken to be 2.25. These parameters lead to a restraining potential on water that smoothly turns on at 20.5 Å, reaches a well at 21.5 Å with a depth of −0.625 kcal/mol, and then quickly rises to be repulsive beyond 22.0 Å. All protein atoms in the buffer region were harmonically restrained with force constants determined directly from the B factors in the PDB file.[37] Langevin atoms were updated heuristically during the simulation to consistently treat protein groups and water molecules that can switch regions during the simulation. For all simulations, all bonds involving hydrogen were constrained using the SHAKE algorithm.[38]

Nonbonded interactions within the inner region were treated with an extended electrostatics model, in which groups beyond 12 Å interact as multipoles.[39] The entire system was heated gradually to 300 K and equilibrated for ∼150 ps prior to the production simulations. To account for the electrostatics between the atoms in the inner and outer regions and the effect of solvation, the generalized solvent boundary potential (GSBP) approach developed by Im and co-workers was used.[35] The static field due to outer-region atoms, ϕ_s^o, and the reaction field matrix, **M**, were evaluated using Poisson−Boltzmann (PB) calculations with a focusing scheme that places a 56-Å cube of fine grid (0.4 Å) into a larger 132-Å cube of coarse grid (1.2 Å). The inner-region charge density was expressed using the first 20th-order spherical harmonics with a total of 400 basis functions. The membrane environment was treated implicitly using a dielectric model with a dielectric constant of 2.0 and a membrane thickness set to 35 Å. The optimized radii of Roux and Nina[40,41] based on experimental solvation energies of small molecules and the calculated interaction energy with explicit waters were adopted to define the solvent−solute dielectric boundary. Dielectric constants of 1.0 and 80.0 were used for protein and solvent, respectively. Further description of the GSBP approach can be found in the Supporting Information.[32]

C. Simulation Setup for Classical MD Simulations. To investigate the conformational flexibility of Arg82, we carried out unbiased classical MD simulations. The initial structure was first minimized using steepest-descent minimization for 100 steps followed by 6000 steps of adopted basis Newton−Raphson minimization. The structure was then heated to 300 K within 110 ps and equilibrated for 200 ps; the simulation was continued by 20 independent 5-ns-long production runs. For all simulations, a time step of 1 fs was used.

D. Free Energy Simulations. The Δrmsd (root-mean-square deviation) approach allows the free energy landscape between two structures (reactant and product) to be computed by driving the dynamics using the difference in the rmsd between the reactant and product structures. To evaluate the free energy change associated with the movement of Arg82, we define a reactant state in which Arg82 is oriented toward the cytoplasmic side and a product state as the conformer in which Arg82 is oriented toward the extracellular side of the protein.

We performed umbrella-sampling MD simulations using the restraint U_j on the ΔD_{rmsd} order parameter given by

$$U_j = K_{rmsd}(\Delta D_{rmsd} - D_{min})^2 \quad (1)$$

where K_{rmsd} is the force constant and D_{min} is the value around which ΔD_{rmsd} is restrained.[42,43] The ΔD_{rmsd} order parameter is the difference in the rmsd values D of each structure ($\mathbf{X}$) obtained during dynamics from the reference initial cytoplasmic-oriented structure ($\mathbf{X}_{E\text{-}CP}$) and the final extracellular-oriented structure ($\mathbf{X}_{P\text{-}EC}$), given by

$$\Delta D_{rmsd} = D(\mathbf{X}, \mathbf{X}_{P\text{-}EC}) - D(\mathbf{X}, \mathbf{X}_{E\text{-}CP}) \quad (2)$$

The reference structures ($\mathbf{X}_{P\text{-}EC}$ and $\mathbf{X}_{E\text{-}CP}$) were obtained from the classical MD simulations described in section IIC. We generated 17 structures with a ΔD_{rmsd} step of 0.2 Å between the two reference structures, such that we had a total of 19 umbrella

Table 1. Distance between the Carboxyl Groups of Asp85 and Asp212 in Various Crystal Structures[a]

intermediate state	PDB	Asp85 Oδ2−Asp212 Oδ2 distance (Å)
bR	1C3W[6]	5.1
bR	1QHJ[51]	5.3
K	1IXF[52]	5.1
K	1M0K[27]	5.1
L	1O0A[49]	5.1
L	1UCQ[16]	5.1
early M	1P8H[53]	5.0
early M	1M0M[54]	4.7
late M	1CWQ[13]	4.3
late M	1IW9[12]	4.4
N	1P8U[55]	4.4
O	1X0I[56]	4.2

[a] See also Figure 3.

sampling windows. For each ΔD_{rmsd} step, we equilibrated the structure for 160 ps by gradually decreasing the force constant from 250 to 50 kcal/(mol·Å^2) in five steps of 20 ps each and continued with 3 ns of production run to ensure the convergence of the calculations.

The time evolution of the ΔD_{rmsd} reaction coordinate was collected from the last 2 ns of the MD trajectory, which were shown in plots to be converged. The potential of mean force (PMF) was constructed from the obtained time evolution of ΔD_{rmsd} reaction coordinate using the weighted histogram analysis method (WHAM).[44,45]

III. RESULTS

To investigate the response of the Arg82 side chain to the transfer of a proton from the Schiff base to Asp85, we performed 20 independent MD simulations on an M-like model (Schiff base and Asp85 neutral) derived from the crystal structure of ref 27 (red structure in Figure 2), as described above. We then computed the free energy for the movement of the Arg82 side chain from the location close to Asp85/Asp212 to the location where it interacts closely with the PRG (blue structure in Figure 2).

A. Classical MD Simulations. Fifteen of the 20 independent MD simulations (Sim1−Sim15) starting from the M-like conformer indicated Arg82 in the cytoplasmic orientation toward the Schiff base region. Arg82 reoriented toward the PRG in five simulations (Sim16−Sim20). The new geometry sampled by Arg82 in the last five MD simulations is similar to that observed in a late-M state crystal structure[13] (blue structure in Figure 2). The movement of Arg82 toward the PRG is coupled with breaking of hydrogen bonds of the hydrogen-bonded clusters at both the Asp85/Asp212 and Glu194/Glu204 sides (Figure 5).

1. Dynamics of the Hydrogen-Bonded Network. The bR active site in its resting state is characterized by a pentagonal hydrogen-bonded network (HBN) consisting of retinal, Asp85/212, and three water molecules (w402, w401, and w406) as shown in Figures 3 and 5a. This HBN is present in the starting structure of the MD simulations. Note, however, that, in contrast to its condition in the bR resting state, Asp85 is protonated in the M-like conformer (Figure 5a), which is the starting structure for the 20 MD simulations. This protonation change weakens the HBN, and during the dynamics of the M-like conformer, the

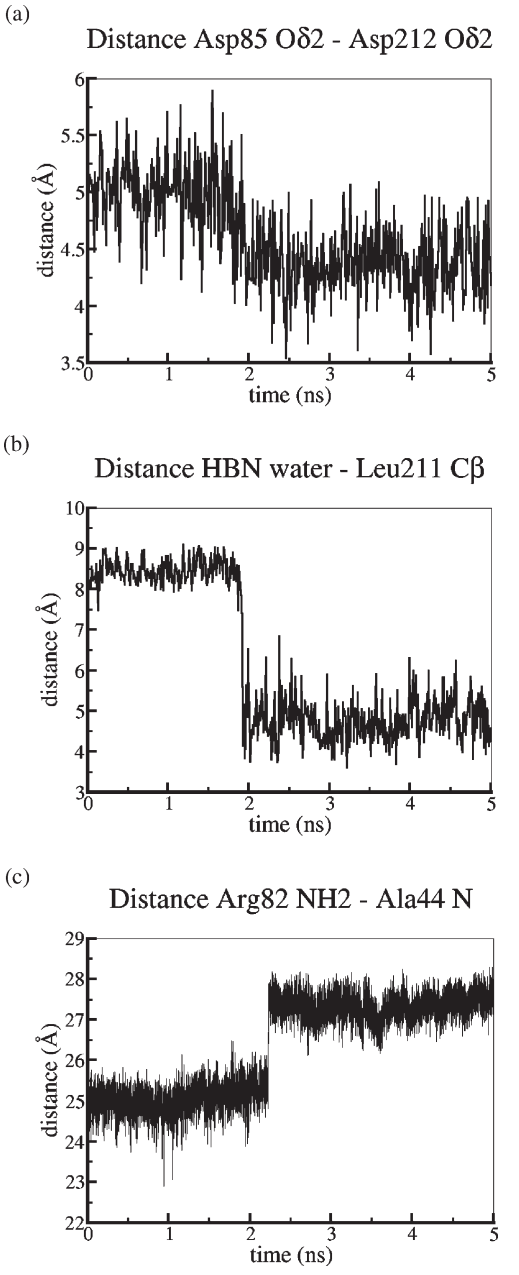

Figure 4. Time series of (a,b) selected distances between groups that participate in the HBN and (c) the movement of the Arg82 side chain relative to a fixed backbone atom.

HBN is severely perturbed. The pentagonal structure is broken, and two water molecules move toward Asp212 and Tyr57, where they form a cluster of H-bonds with Asp212, Tyr57, and Arg82 (Figure 5b). In this M-like geometry, Asp212 has three H-bonds with water molecules, whereas Asp85 forms H-bonds only with water w402. On average, the distance between Asp85 and w402 decreases by 0.1 Å during the dynamics (i.e., the H-bond becomes stronger than in the bR resting state). The observation of stronger H-bonding between Asp85 and w402 is consistent with expectations from IR experiments that protonation of Asp85 is associated with a shift toward higher frequencies of the spectral fingerprint corresponding to water H-bonding of Asp85.[46] In the five simulations where the Arg82 side chain

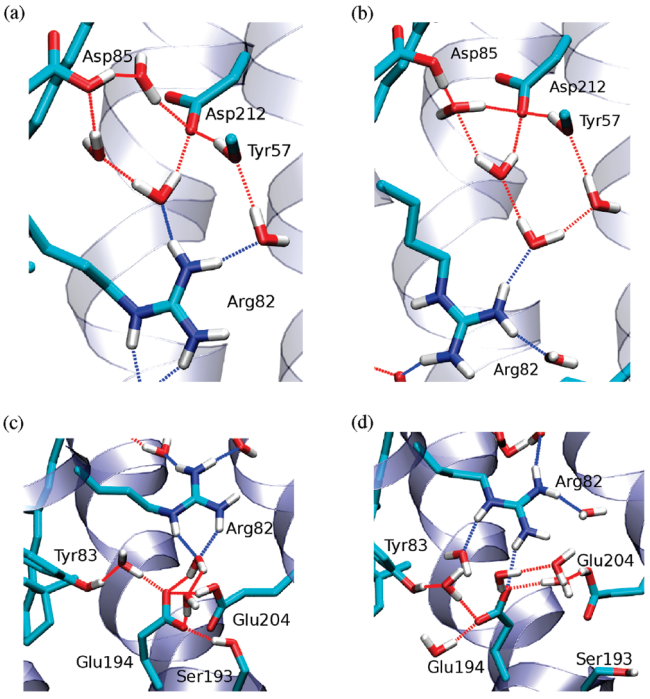

Figure 5. Close view of H-bonding interactions perturbed by the movement of Arg82. (a) HBN consisting of Asp85, Asp212, Arg82, w401, w402, and w406 at the beginning of the simulation; (b) HBN in the extracellular orientation of Arg82 at the end of the simulation; (c) PRG region with three water molecules and Glu194 and Glu204 pointing toward each other at the beginning of the simulation; and (d) PRG region with Glu194 rotated away from Glu204 at the end of Sim16−Sim20.

moves toward the PRG (Sim16−Sim20), the two moving water molecules are closer to Tyr57 by ∼3.5 Å compared to their positions in the 15 simulations in which Arg85 remains oriented toward Asp85/Asp212.

The distance between the carboxyl oxygen atoms of Asp85 and Asp212 appears to be correlated with the structural stability of the HBN. In the crystal structures of the bR, K, and L intermediate states in which the HBN is present, the distance between Asp85 and Asp212 is 5.1−5.3 Å. In contrast, in crystal structures of the second half of the photocycle (late-M, N, and O intermediate states), in which the HBN is disrupted, the distance between Asp85 and Asp212 is 4.2−4.4 Å (Table 1). In the geometry-optimized structure used as the starting point for the 20 independent simulations, the distance between Asp85 and Asp212 is 5.0 Å (Figure 4). In the five simulations where Arg82 reorients from the cytoplasmic to the extracellular configuration, the distance between Asp85 and Asp212 decreases gradually to 4.3 Å at the same time as the HBN is disrupted (Figure 4a). Therefore, the observation that reorientation of Arg82 toward the PRG in the M-like conformer is accompanied by stronger H-bonding between Asp85 and water and a decrease of the Asp85···Asp212 distance is consistent with the change of the Asp85···Asp212 distance indicated by the crystal structures of the bR, K, L, and M intermediate states.

In Figure 4, we compare the distance between the Oδ2 atoms of Asp85 and Asp212 with the distance between a water molecule and the Cβ atom of Leu211 for one of the simulations. The water molecule was part of the HBN at the beginning of the simulation. We use the Cβ atom of Leu211 as a reference because Leu211 is

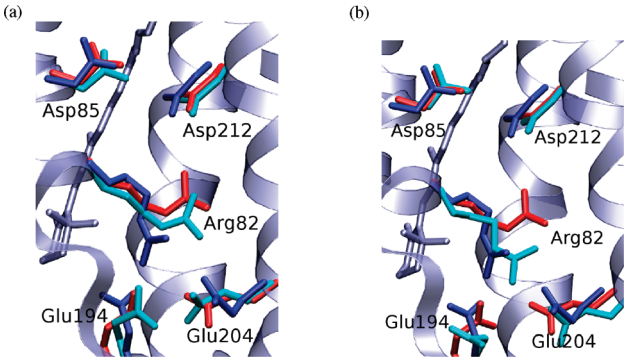

Figure 6. Location of the Arg82 side chain in simulations and in crystal strucures. Selected amino acids are shown at the (a) beginning and (b) end of a simulation in which the Arg82 side chain moved toward the extracellular side (green). The L-state structure 1UCQ[16] is shown in red, and the late-M state structure 1CWQ[13] is in blue.

positioned along the path between Asp85/Asp212 and the PRG (see the Supporting Information) and, during the simulation, it moves very little (∼0.2 Å) as compared to the movement of the water molecules. The water molecule chosen for monitoring the distances was not the same for all graphs because water molecules exchanged locations in the beginning of the simulations. The decrease of the distance between the water molecule and Leu211 occurs at the same time as the decrease of the distance between the carboxyl groups of Asp85 and Asp212 (Figure 4). This movement of the water molecule corresponds to the disruption of the HBN that reduces the number of H-bonding partners for Asp85 and, thus, results in a stronger bond to Asp212 through the single water molecule that remains between Asp85 and Asp212 after the HBN is perturbed.

Movement of Arg82. Within the initial 300 ps of Sim15−Sim20, the disruption of the HBN is followed by the movement of the Arg82 side chain toward the extracellular side within 50 ps (Figure 5a,b). The movement of Arg82 is reversed in one of these trajectories (Sim15) after 200 ps. In the other five trajectories (Sim16−Sim20), the Arg82 side chain remains oriented toward the extracellular side. To illustrate the movement of the Arg82 side chain, we monitor the distance between the backbone N atom of Ala44 (see also the Supporting Information) and the NH1 atom of the Arg82 side chain. Ala44 is part of the immobile part of the protein. The Ala44···Arg82 distance changes from ∼25 Å when the Arg82 side chain is in a cytoplasmic position to ∼27.5 Å when Arg82 reorients toward the PRG (Figure 4).

Structural Changes in the PRG Region. The movement of the Arg82 side chain toward the PRG induces structural changes of the side chains of Glu194, Glu204, and Ser193 (Figure 5c,d). The carboxyl group of Glu194 reorients toward Tyr83, whereas the carboxyl group of Glu204 remains in its original location. The movement of Glu194 leads to an increase of the distance between the Glu194 and Glu204 carboxyl groups in three of the five trajectories in which Arg82 moves toward the EC side (Sim18−Sim20) (Figure 5c,d). In the remaining two trajectories (Sim16 and Sim17), the reorientation of the carboxyl group of Glu194 is smaller, and the distance between the carboxyl groups of Glu194 and Glu204 remains unchanged. The locations of the Glu194 and Glu204 side chains before and after the Arg82 movement are very similar to those indicated by the L-[16] and late-M-state structures,[13] respectively (Figure 6). This suggests

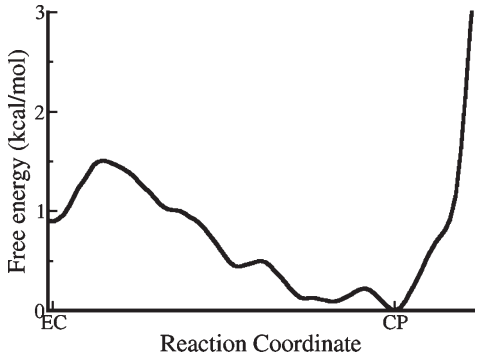

Figure 7. Free energy profile from the Δrmsd calculation with decreased force constant. CP denotes the initial (cytoplasmic) conformation, where Arg82 points toward the Schiff base region, whereas EC denotes the extracellular conformation of Arg82, pointing toward Glu194/204.

that our MD simulations appear to capture the structural changes of the PRG indicated by the crystal strutures. A similar observation was made performing microscopic QM/MM pK_a calculations using a thermodynamic integration within the dual-topology single-coordinate approach. The structural changes during the titration simulations indicate the same movement between the Glu moieties, increasing their distance as a result of the mutual repulsion.[47]

At the beginning of the simulations, the hydroxyl group of Ser193 is H-bonded to the carboxyl group of Glu194 (Figure 5). When the Arg82 side chain reorients toward the PRG, the Ser193 hydroxyl group rotates ∼90° toward the extracellular bulk, away from Glu204. As a result, the Ser193···Glu194 H-bond is broken; Ser193 does not engage in other H-bonds. The reorientation of the Ser193 and Glu194 side chains is observed in all trajectories in which Arg82 moves to the extracellular side, as well as in some of the trajectories where the Arg82 side chain remains in the cytoplasmic orientation.

The Arg movement seems to allow additional waters from the bulk to enter the PRG region. We found additional waters penetrating the PRG region in 10 of 20 simulations. However, in those simulations where Arg82 moved to the extracellular side (Sim16−Sim20), about two to four additional water molecules were found at the end of the simulation, whereas the number of water molecules found for the trajectories where the Arg82 side chain retained its cytoplasmic position (Sim1−Sim15) remained almost unchanged.

2. Free Energy Calculations. Figure 7 shows the free energy profile from the Δrmsd simulation for the transition from the cytoplasmic position of Arg82 (CP) to the extracellular position (EC). The free energy was calculated using umbrella sampling, and the obtained data were converted into the potential of mean force (PMF) with WHAM.[44,45] There is a free energy well representing the cytoplasmic position of Arg82 with a broad energy barrier of 1.5 kcal/mol separating this state from the state with Arg82 oriented to the extracellular side. The conformer with Arg82 oriented toward the PRG is 0.9 kcal/mol higher in energy than that in which Arg82 points toward Asp85/Asp212. We also calculated the PMF from the classical MD simulations by recording the Arg82 side-chain position with respect to the Ala44 backbone N atom. The results confirm those from the umbrella-sampling calculations (see the Supporting Information). The rather small free energy barrier (1.5 kcal/mol) for the movement of Arg82 is consistent with the observation that, in the unbiased trajectories (Sim16−Sim20), Arg82 moves toward the PRG within 50 ps of dynamics at 300 K.

IV. DISCUSSION

We have performed classical MD simulations starting from an M-like conformer with protonated Asp85 and deprotonated retinal. The MD simulations indicate that the transfer of the proton from the Schiff base to Asp85 leads to disruption of the HBN around the Schiff base region. This is in agreement with earlier observations from QM/MM proton-transfer computations where water molecules close to Asp85 and Asp212 rearrange after the first proton-transfer step.[48] The transfer of the proton from the Schiff base to Asp85 is associated with a weaker HBN and with movement of Arg82 toward the extracellular side. The free energy barrier for the movement of Arg82 is small, 1.5 kcal/mol. Consistent with the small free energy barrier, we observed movement of Arg82 in five independent MD simulations that severely perturbs the PRG region. Glu194 and Glu204 move apart into locations consistent with those observed in crystal structures of the M state, and additional water molecules enter the PRG cavity. The small free energy barrier for the movement of Arg82 and the rapid movement of Arg82 toward the PRG in five of our unbiased trajectories at 300 K would suggest that Arg82 likely moves toward the PRG immediately after the first proton-transfer step (i.e., in early M).

Recently, we showed that FTIR spectral fingerprints can be consistently reproduced by simulations in which the PRG consists of Glu204 and Glu194 sharing a proton.[32] The simulations discussed here indicate that the movement of Arg82 toward the PRG upon proton transfer from the Schiff base to Asp85 is accompanied by an increase of the distance between the carboxyl groups of Glu194 and Glu204 (Figure 5c,d). The movement of Glu194/Glu204 upon reorientation of Arg82 could help stabilize the proton transiently on one of the Glu amino acid residues, which would dramatically alter the proton affinity; that is, the proton would be less stable in this new geometry, resulting in a release of the proton to the bulk. This could allow further structural rearrangements, with Arg82 completing the movement to the extracellular side.

■ ASSOCIATED CONTENT

Supporting Information. Additional results for the charges on retinal and free energy calculations. This information is available free of charge via the Internet at http://pubs.acs.org/.

■ AUTHOR INFORMATION

Corresponding Author
*E-mail: marcus.elstner@kit.edu.

■ ACKNOWLEDGMENT

This work was supported in part by the Deutsche Forschungsgemeinschaft through Forschergruppe 490. A.-N.B. was supported by the National Institutes of Health (grants No. GM74637 and No. GM68002).

REFERENCES

(1) Oesterhelt, D.; Stoeckenius, W. *Nature: New Biol.* **1971**, *233*, 149–152.
(2) Oesterhelt, D.; Stoeckenius, W. *Proc. Natl. Acad. Sci. U.S.A.* **1973**, *70*, 2853–2857.
(3) Aton, B.; Doukas, A. G.; Callender, R. H.; Becher, B.; Ebrey, T. G. *Biochemistry* **1977**, *16*, 2995–2999.
(4) Doig, S. J.; Reid, P. J.; Mathies, R. A. *J. Phys. Chem.* **1991**, *95*, 6372–6379.
(5) Lanyi, J. K. *Biochim. Biophys. Acta* **1993**, *1183*, 241–261.
(6) Luecke, H.; Schobert, B.; Richter, H.-T.; Cartailler, J.-P.; Lanyi, J. K. *J. Mol. Biol.* **1999**, *291*, 899–911.
(7) Schobert, B.; Cupp-Vickery, J.; Hornak, V.; Smith, S. O.; Lanyi, J. K. *J. Mol. Biol.* **2002**, *321*, 715–726.
(8) Kandori, H.; Yamazaki, Y.; Shichida, Y.; Raap, J.; Lugtenburg, J.; Belenky, M.; Herzfeld, J. *Proc. Natl. Acad. Sci. U.S.A.* **2001**, *98*, 1571–1576.
(9) Bondar, A.; Fischer, S.; Suhai, S.; Smith, J. *J. Phys. Chem. B* **2005**, *109*, 14786–14788.
(10) Hayashi, S.; Tajkhorshid, E.; Schulten, K. *Biophys. J.* **2002**, *83*, 1281–1297.
(11) Matsui, Y.; Sakai, K.; Murakami, M.; Shiro, Y.; Adachi, S.; Okumura, H.; Kouyama, T. *J. Mol. Biol.* **2002**, *324*, 469–481.
(12) Takeda, K.; Matsui, Y.; Kamiya, N.; Adachi, S. .; Okumura, H.; Kouyama, T. *J. Mol. Biol.* **2004**, *341*, 1023–1037.
(13) Sass, H. J.; Büldt, G.; Gessenich, R.; Hehn, D.; Neff, D.; Schlesinger, R.; Berendzen, J.; Ormos, P. *Nature* **2000**, *406*, 649–653.
(14) Lanyi, J. K.; Schobert, B. *J. Mol. Biol.* **2007**, *365*, 1379–1392.
(15) Lanyi, J. K.; Schobert, B. *J. Mol. Biol.* **2003**, *328*, 439–450.
(16) Kouyama, T.; Nishikawa, T.; Tokuhisa, T.; Okumura, H. *J. Mol. Biol.* **2004**, *335*, 531–546.
(17) Royant, A.; Edman, K.; Ursby, T.; Pebay-Peyroula, E.; Landau, E. M.; Neutze, R. *Nature* **2000**, *406*, 645–648.
(18) Edman, K.; Royant, A.; Larsson, G.; Jacobson, F.; Taylor, T.; Van Der Spoel, D.; Landau, E. M.; Pebay- Peyroula, E.; Neutze, R. *J. Biol. Chem.* **2004**, *279*, 2147–2158.
(19) Facciotti, M.; Rouhani, S.; Burkard, F.; Betancourt, F.; Downing, K.; Rose, R.; McDermott, G.; Glaeser, R. *Biophys. J.* **2001**, *81*, 3442–3455.
(20) Lanyi, J. K.; Schobert, B. *J. Mol. Biol.* **2002**, *321*, 727–737.
(21) Balashov, S. P.; Govindjee, R.; Imasheva, E. S.; Misra, S.; Ebrey, T. G.; Feng, Y.; Crouch, R. K.; Menick, D. R. *Biochemistry* **1995**, *34*, 8820–8834.
(22) Govindjee, R.; Misra, S.; Balashov, S. P.; Ebrey, T. G.; Crouch, R. K.; Menick, D. R. *Biophys. J.* **1996**, *71*, 1011–1023.
(23) Imasheva, E. S.; Balashov, S. P.; Ebrey, T. G.; Chen, N.; Crouch, R. K.; Menick, D. R. *Biophys. J.* **1999**, *77*, 2750–2763.
(24) Song, Y.; Mao, J.; Gunner, M. R. *Biochemistry* **2003**, *42*, 9875–9888.
(25) Subramaniam, S.; Lindahl, M.; Bullough, P.; Faruqi, A. R.; Tittor, J.; Oesterhelt, D.; Brown, L.; Lanyi, J.; Henderson, R. *J. Mol. Biol.* **1999**, *287*, 145–161.
(26) Bondar, A.-N.; Elstner, M.; Suhai, S.; Smith, J. C.; Fischer, S. *Structure* **2004**, *12*, 1281–1288.
(27) Schobert, B.; Cupp-Vickery, J.; Hornak, V.; Smith, S. O.; Lanyi, J. K. *J. Mol. Biol.* **2002**, *321*, 715–726.
(28) MacKerell, A. D., Jr.; Bashford, D.; Bellott, M.; Dunbrack, R. L., Jr.; Evanseck, J. D.; Field, M. J.; Fischer, S.; Gao, J.; Guo, H.; Ha, S.; Joseph-McCarthy, D.; Kuchnir, L.; Kuczera, K.; Lau, F. T. K.; Mattos, C.; Michnick, S.; Ngo, T.; Nguyen, D. T.; Prodhom, B.; Reiher, W. E., III; Roux, B.; Schlenkrich, M.; Smith, J. C.; Stote, R.; Straub, J.; Watanabe, M.; Wiórkiewicz-Kuczera, J.; Yin, D.; Karplus, M., Jr. *J. Phys. Chem. B* **1998**, *102*, 3586–3616.
(29) Jorgensen, W. L.; Chandrasekhar, J.; Madura, J. D.; Impey, R. W.; Klein, M. L. *J. Chem. Phys.* **1983**, *79*, 926–935.
(30) Braiman, M. S.; Bousche, O.; Rothschild, K. J. *Proc. Natl. Acad. Sci. U.S.A.* **1991**, *88*, 2388–2392.
(31) Braiman, M. S.; Mogi, T.; Marti, T.; Stern, L. J.; Khorana, H. G.; Rothschild, K. J. *Biochemistry* **1988**, *27*, 8516–8520.
(32) Phatak, P.; Ghosh, N.; Yu, H.; Cui, Q.; Elstner, M. *Proc. Natl. Acad. Sci. U.S.A.* **2008**, *105*, 19672–19677.
(33) Brünger, A. T.; Karplus, M. *Proteins* **1988**, *4*, 148–156.
(34) Brooks, B. R.; Bruccoleri, R. E.; Olafson, B. D.; States, D. J.; Swaminathan, S.; Karplus, M. *J. Comput. Chem.* **1983**, *4*, 187–217.
(35) Im, W.; Bernèche, S.; Roux, B. *J. Chem. Phys.* **2001**, *114*, 2924–2937.
(36) Schaefer, P.; Riccardi, D.; Cui, Q. *J. Chem. Phys.* **2005**, *123*, 014905.
(37) Brooks, C. L., III; Karplus, M. *J. Mol. Biol.* **1989**, *208*, 159–181.
(38) Ryckaert, J. .; Ciccotti, G.; Berendsen, H. J. C. *J. Comput. Phys.* **1977**, *23*, 327–341.
(39) Steinbach, P. J.; Brooks, B. R. *J. Comput. Chem.* **1994**, *15*, 667–683.
(40) Nina, M.; Beglov, D.; Roux, B. *J. Phys. Chem. B* **1997**, *101*, 5239–5248.
(41) Nina, M.; Im, W.; Roux, B. *Biophys. Chem.* **1999**, *78*, 89–96.
(42) Banavali, N. K.; Roux, B. *J. Am. Chem. Soc.* **2005**, *127*, 6866–6876.
(43) Arora, K.; Brooks, C. L., III. *Proc. Natl. Acad. Sci. U.S.A.* **2007**, *104*, 18496–18501.
(44) Kumar, S.; Bouzida, D.; Swendson, R. H.; Kollman, P. A.; Rosenberg, J. M. *J. Comput. Chem.* **1992**, *13*, 1011–1021.
(45) Boczko, E. M.; Brooks, C. L., III. *J. Phys. Chem.* **1993**, *97*, 4509–4513.
(46) Tanimoto, T.; Furutani, Y.; Kandori, H. *Biochemistry* **2003**, *42*, 2300–2306.
(47) Goyal, P.; Ghosh, N.; Phatak, P.; Clemens, M.; Gaus, M.; Elstner, M.; Cui, Q., manuscript submitted.
(48) Bondar, A. .; Suhai, S.; Fischer, S.; Smith, J. C.; Elstner, M. *J. Struct. Biol.* **2007**, *157*, 454–469.
(49) Lanyi, J. K.; Schobert, B. *J. Mol. Biol.* **2003**, *328*, 439–450.
(50) Bondar, A.-N.; Baudry, J.; Suhai, S.; Fischer, S.; Smith, J. C. *J. Phys. Chem. B* **2008**, *112*, 14729–14741.
(51) Belrhali, H.; Nollert, P.; Royant, A.; Menzel, C.; Rosenbusch, J. P.; Landau, E. M.; Pebay-Peyroula, E. *Structure* **1999**, *7*, 909–917.
(52) Matsui, Y.; Sakai, K.; Murakami, M.; Shiro, Y.; Adachi, S.-I.; Okumura, H.; Kouyama, T. *J. Mol. Biol.* **2002**, *324*, 469–481.
(53) Schobert, B.; Brown, L. S.; Lanyi, J. K. *J. Mol. Biol.* **2003**, *330*, 553–570.
(54) Lanyi, J. K.; Schobert, B. *J. Mol. Biol.* **2002**, *321*, 727–737.
(55) Schobert, B.; Brown, L. S.; Lanyi, J. K. *J. Mol. Biol.* **2003**, *330*, 553–570.
(56) Okumura, H.; Murakami, M.; Kouyama, T. *J. Mol. Biol.* **2005**, *351*, 481–495.